In Situ Grown Nanohydroxyapatite Hybridized Graphene Oxide: Enhancing the Strength and Bioactivity of Polymer Scaffolds

Dongying Li,[†] Meigui Chen,[†] Wenmin Guo, Pin Li, Haoyu Wang, Wenhao Ding, Mengqi Li,* and Yong Xu*

Cite This: *ACS Omega* 2022, 7, 12242−12254

Read Online

ACCESS | Metrics & More | Article Recommendations

ABSTRACT: Graphene oxide (GO) and nanohydroxyapatite (nHA) are usually used for improving the strength and bioactivity of polymer scaffolds. However, due to the nano-aggregation effect, these applications often face the problems of uneven dispersion and poor interface bonding. In this work, their hybrids (GO@nHA) were constructed by combining chemical modification and in situ growth methods, realizing the perfect combination of nHA and GO. First, the functionalization of GO was realized through oxidative self-polymerization of dopamine (DA), and the product was denoted GO@DA. Furthermore, the in situ growth of nHA on GO@DA was induced by hydrothermal reactions to prepare GO@nHA hybrids. Then, the obtained hybrid was added to the polymer matrix, and a composite scaffold was prepared through a selective laser sintering process. The results demonstrated that with the addition of GO@DA and GO@nHA, the ultimate strength was increased to 16.8 and 18.6 MPa, respectively, which is 66 and 84% higher than the 10.1 MPa of the polylactic acid (PLA) scaffold. In addition, composite scaffolds exhibited good biomineralization ability in vitro and also promoted the adhesion and proliferation of MG63 cells.
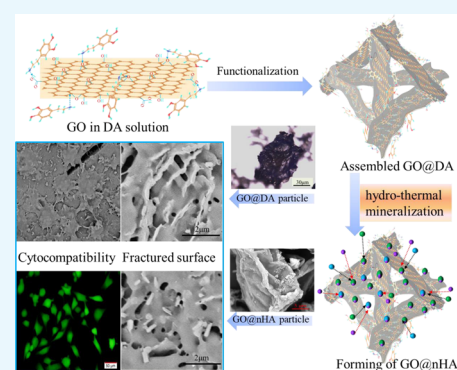
1. INTRODUCTION

There are tens of millions of patients suffering from bone defects every year, so implants and biomaterials for bone defect repair are urgently needed worldwide.[1] Polylactic acid (PLA), a degradable implant material approved by FDA, has the advantages of a wide range of raw materials, good biocompatibility, and good processability, while it has the disadvantages of a lack of bioactivity and insufficient mechanical properties.[2,3] Hydroxyapatite (HA) is a bioceramic with good osteoconductivity and osteoinductivity, and its calcium−phosphorus atomic molar ratio is consistent with the inorganic components of human bone (1.667).[4] In addition, the hydroxyl groups with polar effects on the surface can be associated with cell membrane proteins through hydrogen bonding, showing good biocompatibility.[5] At present, the introduction of HA into the PLA matrix using the idea of a material composite has been adopted by researchers. For example, Lu et al.[6] found that the addition of HA effectively improved the tensile strength and tensile modulus of PLA composite films. Zhang et al.[7] reported that the elongation at break of PLA increased from 4.24 to 8.79% after adding HA nanorods. However, there are still many problems to be resolved urgently, such as dispersion, interface compatibility, and mechanical stability.

Taking into account the unique advantages of bioceramics and polymer materials, the use of suitable methods to organically composite these two biomaterials is expected to overcome the above problems and achieve complementary performance. Graphene oxide (GO), which has a layered structure and excellent properties similar to graphene, shows great advantages and application potential in enhancing the mechanical properties of composite materials.[8,9] More importantly, there are many oxygen-containing groups such as carboxyl, carbonyl, and hydroxyl on the plane and edge of carbon atoms, which can interact with the polymer (such as PLA) and bioceramic (such as HA) through noncovalent bonding.[10,11] Therefore, GO is expected to become a link between polymers and bioceramics, improve the interface compatibility of composite materials, and realize the organic combination of polymers and bioceramics.

The "in situ growth" technology is to induce "nucleation" and "crystal growth" of inorganic particles on a matrix under specific conditions by the nature of the material itself, and it is a new way to prepare composite materials.[12] According to reports, dopamine (DA) is a green modifier with mussel-like
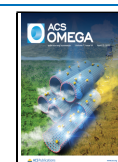
foot mucin catechol and amine functional groups.[13] Under alkaline conditions, $-O^-$ groups will form on dopamine after deprotonation, thereby adsorbing positively charged calcium ions (Ca^{2+}) through chelation.[14−16] Enrichment of Ca^{2+} accelerates the nucleation of HA and further promotes the in situ growth of HA through electrostatic adsorption.[17,18] Therefore, if dopamine is used to functionalize GO, it is expected to combine the chelating function of catechol groups and the electrostatic effect of oxygen-containing functional groups. The synergistic effect of these two mechanisms will quickly promote the enrichment of Ca^{2+} and induce the "in situ growth" of nanohydroxyapatite (nHA), thereby obtaining a GO@nHA multicomponent complex. Furthermore, we expect that by introducing GO@nHA into the PLA matrix by a suitable method, an artificial composite bone scaffold with good biological activity and mechanical properties will be obtained.

This work has two main contents: one of which is tantamount to constructing a hybrid of nHA and GO (GO@nHA) by combining chemical modification and in situ growth methods. The other is to develop polymer scaffolds containing GO@nHA through a laser additive manufacturing process and evaluate the impact of the new hybrid on the performance of polymer scaffolds. Specifically, the composition and structure of the hybrid were characterized by Raman, X-ray photoelectron spectroscopy (XPS), X-ray diffraction (XRD), and scanning electron microscopy (SEM) techniques. Moreover, the potential reaction mechanism in the process of dopamine-functionalized GO was also discussed, and the in situ growth mechanism of nHA was further analyzed. Besides, the mechanical properties of the composite scaffold and the cytocompatibility of scaffold material were also analyzed.

2. MATERIALS AND METHODS

2.1. Materials. Polycaprolactone pellets (PCL, Capa 6400; Perstorp, Sweden) with a melting point of 60 °C, a molecular weight of about 40 000, and a density of 1.146 g·mL^{-1} at 25 °C were selected as the raw material. After further crushing and sieving (300 meshes), PCL powder with an average particle size of about 48 μm was obtained. PLA pellets (4032D, Nature Works) with an average molecular weight of 3.7×10^5 g·mol^{-1} were treated in the same way to obtain PLA powder. Dopamine hydrochloride (DA-HCl, 99%) and tris-hydroxymethylaminomethane hydrochloride (Tris−HCl, pH = 8.5, 99%) were purchased from Aladdin Biotechnology Company (Shanghai, China). Graphene oxide (GO, 99.9%) was provided by Tanfeng Technology (Shenzhen, China). Diammonium phosphate ((NH_4)$_2$HPO$_4$), calcium nitrate tetrahydrate (Ca(NO$_3$)$_2$·4H$_2$O), and ammonia solution were obtained from Sinopharm Group Chemical Reagent Co., Ltd. (China). Without instructions, all reagents were used directly as received.

2.2. Dopamine Functionalization of GO. In this work, GO was used as a reinforcing phase to enhance the mechanical properties of the polymer composite matrix (a mixture of PLA and PCL at a ratio of 1:1, denoted PLPC). Moreover, dopamine was used for functionalizing GO to further enhance interface interactions. Specifically, first, dissolve dopamine in a 0.1 mM Tris−HCL solution and control its final concentration to 2 mg/mL. Subsequently, GO was added under vigorous magnetic stirring, and its concentration was kept at 1 mg/mL, followed by vigorous stirring for 30 min to achieve uniform dispersion of GO. Then, the frequency was adjusted to gentle

stirring and the reaction was continued at room temperature for 5 h. Finally, the obtained suspension was centrifuged (6000 rpm) and then the precipitate was placed in a constant-temperature vacuum drying oven at 60 °C overnight to obtain dopamine-functionalized graphene oxide powder (denoted GO@DA). The structure of GO@DA was evaluated by confocal micro-Raman spectroscopy (JR HR800, Paris, France). Fourier transform infrared (FTIR, Tianjin Gangdong Technology Co., Ltd., China) spectroscopy was used to evaluate the changes in the chemical bond structure of GO before and after modification. In addition, X-ray photoelectron spectroscopy (XPS, Thermo Fisher-VG Scientific) was utilized to further analyze the chemical composition of GO@DA.

2.3. GO@nHA Preparation and Characterization. Considering the osteoinductive ability of scaffold material, GO@DA was further placed in a 50 mL stainless steel hydrothermal synthesis reactor (Qiu Zuo Technology, Shanghai, China) containing a mineralized precursor solution, and then, the reactor was placed in a heating furnace at 120 °C for 10 h. After natural cooling, the solution in the reactor was removed, and the GO@nHA complex was obtained by centrifugation and drying. Among them, the main components of the precursor solution include a phosphorus source such as (NH_4)$_2$HPO$_4$ and a calcium source such as Ca(NO$_3$)$_2$·4H$_2$O, and the molar ratio of calcium to phosphorus is controlled to 1.67. Under hydrothermal conditions, violent molecular motion and strong intermolecular interactions induce the inorganic component of bone nanohydroxyapatite (nHA) to "nucleate" and "crystal growth" on the GO@DA matrix, forming the GO@nHA complex. It expects that nHA grown in situ will be perfectly combined with GO. The microscopic morphology of prepared GO@nHA was characterized by SEM, and its elementary composition was analyzed by EDS. Moreover, the micro three-dimensional network structure of the GO@DA complex was observed with an ultra-depth-of-field microscope. Moreover, XPS was used to detect the spectrum of GO@nHA and focused on detecting the calcium peak of nHA formed in situ.

2.4. Scaffold Preparation and Characterization. Prior to the preparation of scaffolds, composite powders for selective laser sintering were prepared. Specifically, a predetermined amount of the PLPC matrix was added to ethanol solution to prepare a homogeneous suspension. Subsequently, the previously prepared GO@DA or GO@nHA were added to the newly prepared polymer suspension (control the amount of GO to 2 wt %) and magnetically stirred for 30 min. After mixing, powders of PLPC/GO@DA and PLPC/GO@nHA were obtained by centrifugal washing and vacuum drying at 60 °C for 12 h. Finally, the above composite powders were introduced into a selective laser sintering (SLS) system independently built by the research group to complete the preparation of PLPC/GO@DA and PLPC/GO@nHA scaffolds. Specifically, built-in CAD software was used to design the porous scaffold model, and then, the file was converted into the STL format and sliced to generate laser processing objects. Subsequently, the composite powder was sintered layer by layer by laser energy. The constant processing parameters during processing are as follows: laser power, 5.4 W; laser rate, 180 mm/s; powder layer thickness, 0.1 mm; and scanning spacing, 1.00 mm. Meanwhile, PLA scaffolds were prepared in the same manner as a control.

To evaluate the dispersion of GO@DA and GO@nHA fillers in the polymer matrix and the preservation of their
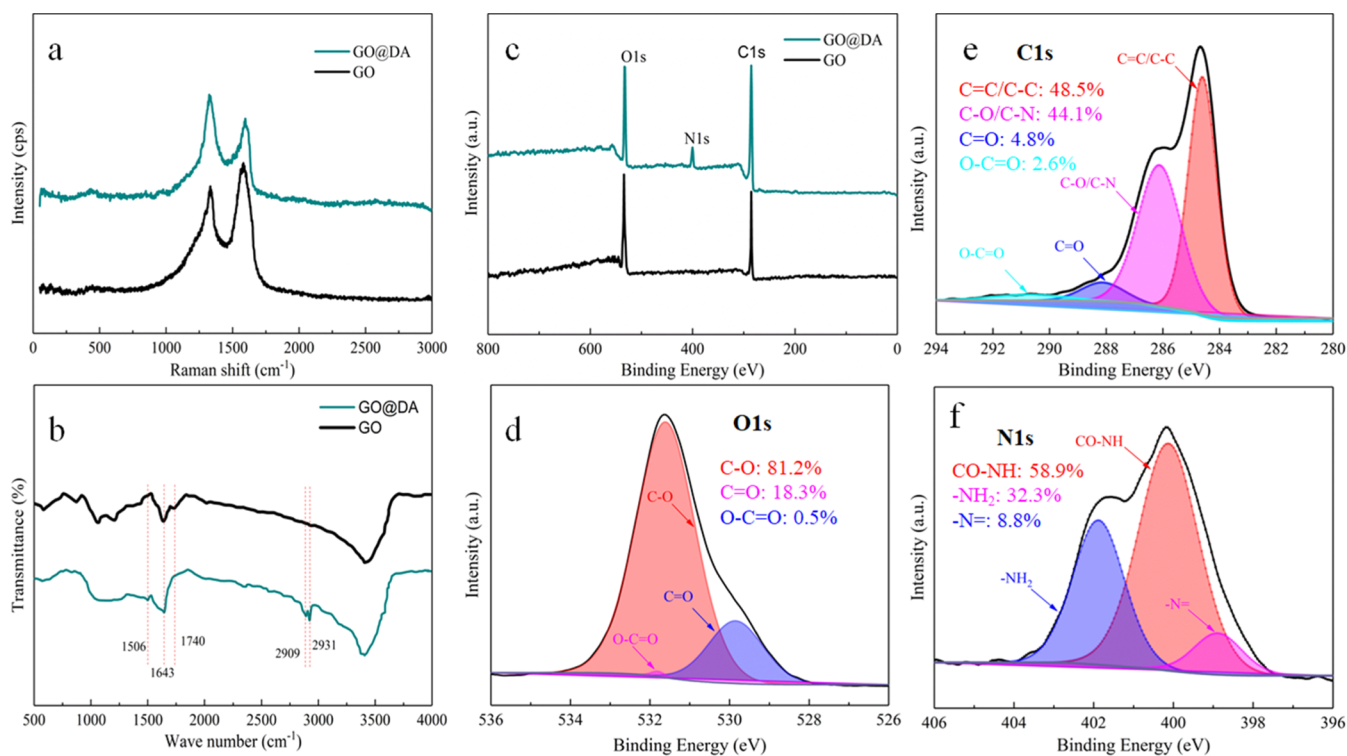
Figure 1. Characterization of GO@DA and GO. (a) Raman spectra. In comparison, the G band of GO@DA became wider and moves up to 1600 cm^{-1}, and the intensity of the D band at around 1334 cm^{-1} increased significantly. This indicated that GO@DA has more defect sites but still retains the inherent planar sp^2 structure of GO. (b) FTIR spectra. It was worth noting that there is a vibration absorption peak attributed to the amide group (N−H) at 1506 cm^{-1}, confirming that dopamine has successfully functionalized GO. Encouragingly, the C═C vibrational stretching absorption peak attributed to sp^2 hybridization was still detected in the spectrum, indicating that dopamine functionalization has not destroyed the inherent carbon chain structure of GO. XPS investigation: (c) wide survey scans and high-resolution (d) O 1s, (e) C 1s, and (f) N 1s spectra of GO@DA. The appearance of C−N may be attributed to the ring-opening reaction during modification of dopamine and reduction of GO.

inherent structure, the micromorphology of the prepared scaffolds was analyzed through SEM tests. Moreover, to evaluate the impact of fillers on the mechanical properties of scaffolds, compression tests were performed using universal testing equipment (Metes Industrial Systems Co., Ltd., China). The size of the sample used for the compression test was $\varphi 3 \times 5$ mm^3. The loading rate was set to 0.5 mm/min. Each group contained no less than three replicate samples to calculate the average and standard deviation.

2.5. Biomineralization. The bioactivity of the scaffold was evaluated by detecting the formation of bonelike apatite after immersion in the simulated body fluid (SBF). First, SBF was prepared according to the method of Liu et al.,[19] and its inorganic ion composition was controlled to be approximately the same as that of human plasma. Subsequently, PLPC, PLPC/GO@DA, and PLPC/GO@nHA scaffolds were immersed in SBF (pH = 7.4), maintaining a solid/liquid ratio of 0.1 g/mL and incubating at 37 °C for 14 days. During the soaking process, the SBF solution was renewed every other day. After reaching the set incubation time, scaffolds were taken out and carefully rinsed with distilled water several times to remove mineral salt components adhering to the surface of the scaffolds. After cleaning, all scaffolds were dried to a constant weight in an oven at 60 °C, then subjected to gold sputtering at a current of 10 mA for 120 s, and observed with an SEM equipped with EDS to determine the formation of apatite.

2.6. Cell Culture. Considering that the human osteosarcoma MG-63 cell line has the ability of bone matrix synthesis and mineralization, it is generally considered that it can be used as an osteoblast model with phenotypic characteristics of human osteoblasts. Therefore, MG-63 cells (American Type Culture Collection, Manassas, VA) were chosen to detect the cytocompatibility of materials. They were cultured in Dulbecco's modified Eagle's medium supplemented with sodium pyruvate and 10% FBS plus 1% antibiotic antifungal solution at 37 °C in a humid environment with 5% CO_2. Prior to cell seeding, all scaffolds were cleared by absolute ethanol and sterilized under a UV environment for 1 h. Subsequently, the scaffolds were placed in a 48-well plate to inoculate at a density of 1×10^5 cells/mL and cultured for a predetermined time.

When the predetermined incubation time was reached, the scaffolds were taken out and gently washed with PBS. Subsequently, the adherent cells were fixed with 2.5% glutaraldehyde for half an hour. Finally, they were dehydrated with a graded ethanol series and dried at 37 °C for 6 h. After the moisture was completely removed, perform gold sputtering for SEM observation. In addition, the viability of cells was evaluated by a fluorescent staining assay. In short, at a predetermined incubation time, scaffolds were taken out and washed with PBS. Then, samples were placed in a fresh medium containing calcein-AM and cultured for another 30 min. During this period, a calcein reaction will occur between intracellular esterase and AM, causing the living cells to be stained green. Finally, use a fluorescence microscope to observe the morphology and number of surviving cells (stained with green). Furthermore, to evaluate the effect of scaffold
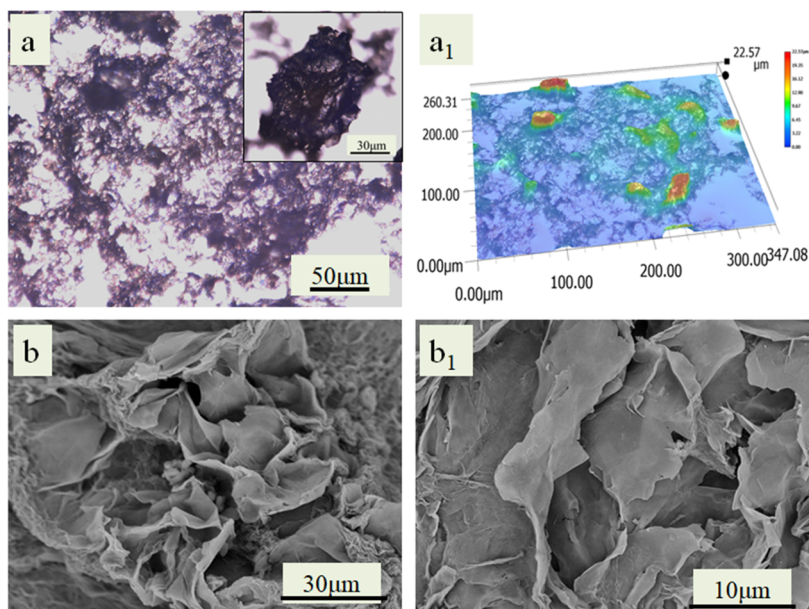
Figure 2. Microscopic morphology of GO@DA. Ultra-depth-of-field images at low (a) and high magnification (illustration) and surface profile topography (a_1). SEM images at low (b) and high magnification (b_1). GO@DA presents a spatially interconnected porous network structure.

material in promoting osteogenic differentiation of cells, the alkaline phosphatase (ALP) level of cells after 3 days of culture was detected using the LabAssay ALP kit (Wako, Osaka, Japan). Adherent cells were removed with 0.25% trypsin solution, fixed with 4% paraformaldehyde for 30 min, then washed with PBS and ALP stained according to the protocol. Finally, an inverted microscope (TE2000U, Nikon, Japan) was used to image the stained cells.

2.7. Statistical Analysis. All experimental data involved in quantitative analysis in this study are expressed as mean ± standard deviation. Also, according to different needs, one-way analysis of variance or Student's t-test was selectively used for statistical analysis. If $P < 0.05$, * was used to indicate a significant difference.

3. RESULTS AND DISCUSSION

3.1. Characterization of GO@DA. Raman spectroscopy is a powerful nondestructive tool for characterizing carbonaceous materials, especially for distinguishing the ordered and disordered crystal structures of carbon.[20] In the Raman spectrum of GO (Figure 1a), the peak at about 1584 cm^{-1} (G band) is linked to the vibration of sp^2-bonded carbon atoms in the two-dimensional hexagonal lattice. The peak at about 1334 cm^{-1} (D band) indicated the disorder of GO, which was caused by defects related to vacancies, grain boundaries, and amorphous carbon species. In comparison, the G band of GO@DA became wider and moves up to 1600 cm^{-1}, and the intensity of the D band at around 1334 cm^{-1} increased significantly. This indicated that GO@DA has more defect sites but still retains the inherent planar sp^2 structure of GO.[21] I_D/I_G is the intensity ratio of the D band and G band, where "I" stands for intensity. This ratio can be used to describe the intensity relationship of these two peaks. In general, its larger value indicates more defects in the C atomic crystal. The I_D/I_G of original GO was obtained by calculating the integral area of the D band and G band, which is about 0.87. It was worth noting that DA modification increased the I_D/I_G of GO@DA to 1.05. These results suggested that GO@

DA has more defect sites, which may be attributed to the loss of some oxygen-containing functional groups on the edge or center plane with dopamine modification.[22] Generally speaking, the results of Raman spectroscopy indicated that GO functionalization via dopamine has been successfully implemented.

In addition, the FTIR spectrum of the prepared material was also determined, and the results are shown in Figure 1b. It can be found that there are three typical absorption peaks in the spectrum of GO. One of the absorption peaks is at 1740 cm^{-1}, which is attributed to the stretching vibration of the carboxyl group (COOH) or conjugated carbonyl group (C=O) at the edge of the basal plane.[23] The other absorption peak is caused by C=C (aromatic) vibrational stretching of sp^2 hybridization at 1643 cm^{-1}. In addition, there is another absorption peak attributed to νC−O, which appears at 1050 cm^{-1}. In the GO@DA spectrum, the characteristic peaks near 1740 and 1050 cm^{-1} weakened or even disappeared, which is due to the loss of some oxygen-containing functional groups during dopamine functionalization.[24] It was worth noting that there is a vibration absorption peak attributed to the amide group (N−H) at 1506 cm^{-1}, confirming that dopamine has successfully achieved the functionalization of GO. Furthermore, in the GO@DA spectrum, the absorption bands of methylene (CH$_2$) appear at around 2909 and 2931 cm^{-1}, which may be attributed to the reduction of GO and the functionalization of dopamine.[25] Encouragingly, the C=C vibrational stretching absorption peak attributed to sp^2 hybridization was still detected in the spectrum, indicating that dopamine modification has not destroyed the inherent carbon chain structure of GO.[26] In spectra of both GO and GO@DA, a broad diffraction peak belonging to νOH was detected at 3400 cm^{-1}. On the one hand, it might be caused by moisture absorbed during the sample preparation process. On the other hand, GO and GO@DA themselves contain a large number of hydroxyl groups. These results provide reliable evidence to confirm the functionalization of dopamine and partial reduction of GO. The partially reduced graphene oxide is expected to combine
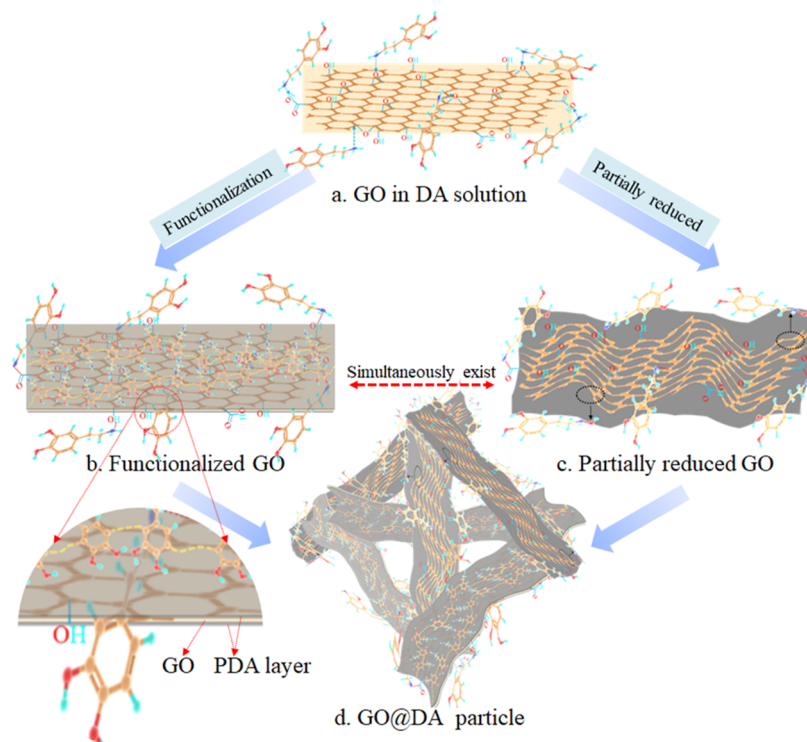
Figure 3. Schematic illustration of the preparation of GO@DA particles. (a) Potential reaction sites between GO and dopamine. (b) Dopamine-functionalized GO. (c) Deoxygenation reduction of GO. (d) Formation of porous GO@DA particles.

the properties of GO and graphene; that is, it has both good biocompatibility and excellent mechanical properties. Therefore, the introduction of GO@DA may have a positive impact on the mechanical and biological properties of the polymer matrix.

Furthermore, XPS was used to more accurately assess the chemical composition of GO@DA (Figure 1c−f). It can be clearly seen from Figure 1c that the main constituent elements of GO were carbon and oxygen. In comparison, in the GO@DA spectrum, a new N1 absorption peak attributable to dopamine appears near 400 eV, further confirming the success of functionalization. In addition, it was calculated that the C/O ratio on GO@DA after functionalization is about 5.18, which is higher than 2.31 of the original GO. It can be explained by the loss of oxygen-containing functional groups during partial chemical reduction of GO by dopamine.[27] Moreover, GO@DA's high-resolution C 1s, N 1s, and O 1s spectra were fitted to analyze the detailed chemical states of different elements. The spectrum of C 1s fits multiple characteristic peaks, containing sp^2 hybrid carbon (C−C and C═C bonds) centered at the energies of 284.8 and 286.3 eV attributed to the CN bond and CO bond, 288.1 eV corresponding to the C═O bond, and 290.8 eV corresponding to the COOH bond.[28] Among them, the appearance of C−N might be attributed to the ring-opening reaction during modification and reduction of GO via dopamine (see Figure 3). Here, it is expected that the formed C−N covalent bond with stronger bond energy will provide powerful help for enhancing the mechanical properties of composite materials. The N 1s spectra were also fitted to O═C at 529.8 eV, O−C at 531.7 eV, and O−C═O at 531.9 eV.[29] The existence of these oxygen-containing functional groups could be explained by the following two aspects: on the one hand, there were still some oxygen-containing functional groups in partially reduced GO;

on the other hand, the polydopamine modified layer formed by dopamine polymerization was accompanied by a large number of oxygen-containing functional groups. In Figure 1f, the primary amine (−NH$_2$) near 401.9 eV in the N 1s fitting spectrum might be formed during the noncovalent self-assembly process of dopamine.[30] The secondary amine (−NH) at 400.1 eV might be caused by the deoxygenation reaction between −NH$_2$ of dopamine and −COOH of GO during the redox process.[31] The tertiary amine/arylamine (−N═) at 398.9 eV position might be related to the intermediate formed during oxidation and self-polymerization of dopamine.

The microscopic morphology of GO@DA was examined by an ultra-depth-of-field microscope and SEM, as shown in Figure 2. Under a super-depth-of-field microscope, the observed GO@DA presents a spatially interconnected porous network structure (as shown in Figure 2a), in which the illustration in the upper right corner shows an independent three-dimensional porous particle. In addition, the surface profile topography of GO after dopamine treatment was also tested, and the results are shown in Figure 2a$_1$. The SEM results further confirmed that the formed GO@DA has a three-dimensional porous structure, as shown in Figure 2b,b$_1$. It can be seen that GO@DA has surface wrinkles and porous structures formed by stacking of nanosheets. In view of the inherent properties of DA and hydrothermal environment, GO might be locally reduced due to the deoxygenation reaction of oxygen-containing groups. During the formation of GO@DA, some complicated processes will occur, including spontaneous polymerization and cross-linking of DA, chemical/thermal reduction of GO, etc. In this regard, electrostatic interaction, $\pi-\pi$ stacking, and chemical bonding will contribute to the formation of three-dimensional porous GO@DA particles. Among them, electrostatic interaction and chemical adhesion
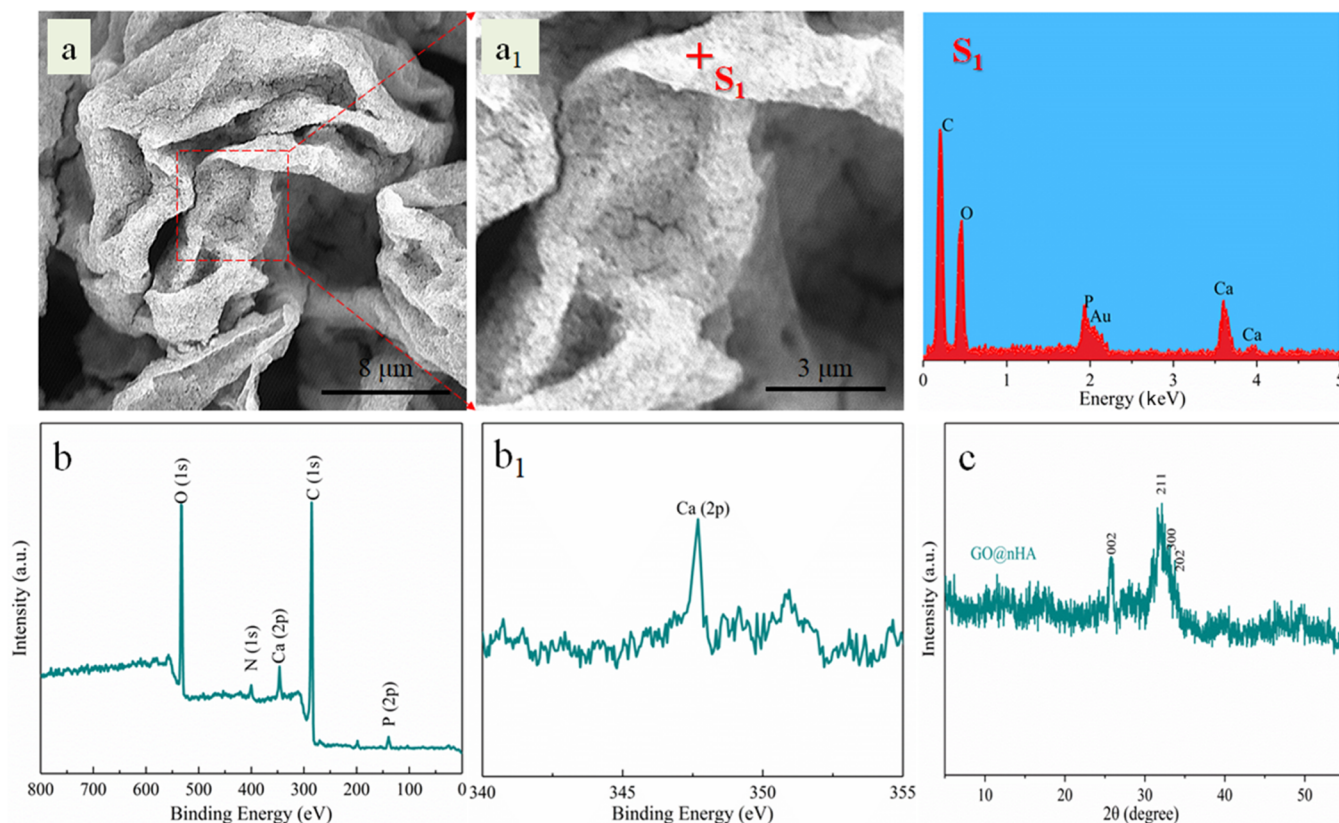
Figure 4. Microscopic morphology and chemical composition of GO@nHA obtained by the hydrothermal reaction. SEM images at low (a) and high (a_1) magnification. After repeated washing steps, nHA was still firmly anchored on GO@DA, indicating that there is a strong interface bond between GO and nHA. XPS spectra: (b) wide survey scans and (b_1) high-resolution Ca (2p). (c) XRD pattern: it confirmed that the product on the surface of GO was nHA.

were the main driving forces of physical/chemical reactions, and $\pi-\pi$ stacking will be the driving force for the formation of porous structures.[32]

3.2. Formation Mechanism of GO@DA. The possible reaction mechanism in the process of dopamine functionalization of GO has been studied, as shown in Figure 3. As we all know, a large number of oxygen-containing functional groups such as epoxy, hydroxyl, and carboxyl groups are distributed on the central plane and edge of the GO nanosheet. Studies have shown that these oxygen-containing functional groups become natural platforms for intermolecular interactions or reactions.[33] Throughout the functionalization process, the potential reaction sites of dopamine with these oxygen-containing functional groups of GO were analyzed, as shown in Figure 3a. Generally, the most likely reaction site was considered to be the epoxy group in the central plane. Potential types of reactions that exist in the process of dopamine functionalization of GO were also discussed. Specifically, a C−N covalent bond with higher bond energy and a more stable structure will be formed through a ring-opening reaction between the amine group of dopamine and the epoxy group of GO. In addition, under alkaline conditions, dopamine undergoes oxidative self-polymerization to form a highly adhesive polydopamine layer, which covers the surface of GO to achieve functionalization.

According to reports, molecules containing amine groups have the ability to remove the oxygen atoms of oxygen-containing functional groups under hydrothermal conditions, thereby achieving a partial reduction of GO.[34] Based on this, it is inferred that dopamine should have the potential of redox

GO. Therefore, the possible mechanism of partial reduction of GO was analyzed, as shown in Figure 3c. In detail, a deoxygenation reaction may occur between the amine group of dopamine and the carboxyl group at the edge of GO to realize local reduction of GO. In this process, although the reduction process achieved by extracting oxygen atoms does not form a new chemical bond structure, it can make a graphene-like structure with stronger mechanical properties appear in the local area of GO. Moreover, partially reduced GO will have a large number of wrinkles in the microscopic morphology, which can achieve faster transfer of the stress at the interface.[35,36] More importantly, a polydopamine layer covering the surface of GO@DA has a large number of benzene ring structures, which promote the assembly of GO@DA nanosheets under the action of strong $\pi-\pi$ bonds to form particles with a porous structure,[37] as shown in Figure 3d. Considering the graphene-like and microspace network structure of GO@DA, as well as the high-efficiency stress transfer ability, it is reasonable to believe that the prepared GO@DA particles have great potential in improving the scaffold's mechanical properties.

3.3. Characterization of GO@nHA. The microscopic morphology of GO@nHA obtained through the hydrothermal reaction was analyzed by SEM, as shown in Figure 4a,a_1. It can be clearly seen that a large number of particles almost uniformly distributed adhere to the surface of GO@DA. Despite repeated washing steps, nHA was still firmly anchored on GO@DA, indicating that there is a strong interface between GO and nHA. It is foreseeable that strong interface
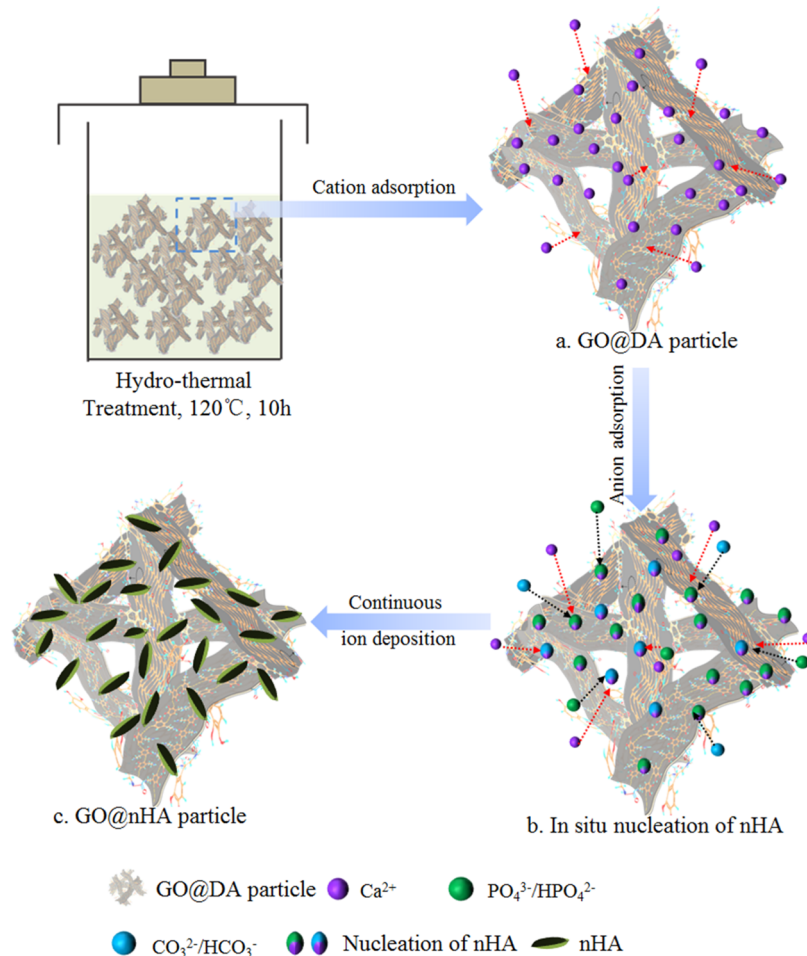
Figure 5. Schematic diagram of the preparation mechanism of GO@nHA composites under hydrothermal conditions. (a) Through the chelation of catechol groups and the adsorption behavior of −COOH or COO− groups, a calcium-rich layer with a large number of Ca^{2+} nucleation sites is formed on the surface of GO@DA. (b) Ca^{2+} nucleation site reacts in situ with the anions in the solution such as PO_4^{3-} and CO_3^{2-} through the electrostatic effect to achieve the nucleation of nHA. (c) Continuous deposition of ions accelerates the in situ growth of nHA, thereby obtaining the GO@nHA composite material.

compatibility will have a significant impact on the improvement of the mechanical properties of the composite scaffold. Combined with the appearance of characteristic peaks of Ca and P in the EDS spectrum, it can be confirmed that these new substances were calcium−phosphorus ceramics. These results indicated that the surface of GO@DA may be covered with a large amount of bonelike apatite (nHA), which was defined as GO@nHA. In addition, the Ca/P ratio (1.58) of bonelike apatite in GO@nHA was calculated by the EDS spectrum, which is slightly lower than that of pure HA (1.67). According to the reports, the apatite in the human body is usually calcium-deficient.[38] In this regard, the chemical composition of bonelike apatite in GO@nHA is closer to human biological apatite, so they are likely to be suitable for the field of bone tissue engineering.

To further confirm the chemical composition and phase of the substances formed on the surface of GO@DA, XPS and XRD tests were also performed, and the results are shown in Figure 4b,c. In the XPS spectrum for the chemical composition inspection, compared with the GO@DA spectrum (Figure 2), new absorption peaks of Ca(2p) and P (2p) appeared near 347 and 150 eV, which correspond to the Ca and P ions of apatite, respectively.[39] The presence of these strong peaks of Ca and P further indicated that the produced substance is HA. In the

WXRD pattern of the phase structure detection, the characteristic diffraction peak of HA (indexed on the spectrum) is also very obvious, as shown in Figure 4c. Obviously, the peaks appearing at 31.9, 32.7°, 33.7, and 25.8° in the diffraction pattern correspond to HA's (211), (300), (202), and (002) reflections (JCPDS card No. 09-0432), showing the typical hexagonal phase characteristic line of HA. This result further confirmed that the substance formed on GO@DA was HA.

3.4. Formation Mechanism of GO@nHA. The mechanism of GO@DA inducing mineralization was also discussed, as shown in Figure 5. On the one hand, graphene oxide has many oxygen-containing groups such as carboxyl, carbonyl, and hydroxyl groups distributed on the carbon atom plane. Studies have shown that its rich oxygen-containing functional groups such as −COOH or COO− can strongly combine with Ca^{2+} ions to achieve nucleation and further induce the in situ growth of biologically beneficial particles such as nHA through electrostatic effects.[40] Although some oxygen-containing functional groups were lost during the partial reduction process, the previous test results confirmed that some oxygen-containing functional groups still exist in the GO@DA structure (Figure 2). Therefore, only from the perspective of graphene oxide, we have reason to believe that GO@DA still has the ability to induce apatite mineralization. Moreover, the huge specific
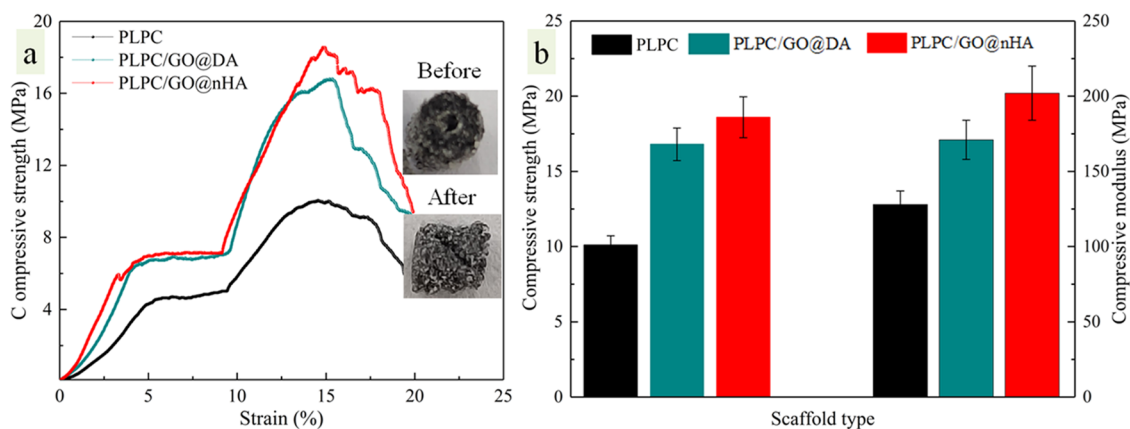
Figure 6. Compression properties tests. (a) Stress−strain curves of different types of samples. The illustrations are digital photos of the scaffold samples before and after the compression test. After the compression test, the scaffold was fractured along 45°. (b) Compressive strength and modulus obtained from the stress−strain curves. With the addition of GO@DA and GO@nHA, the ultimate strength was increased to 16.8 and 18.6 MPa, respectively, which is 66 and 84% higher than that of the PLPC scaffold.
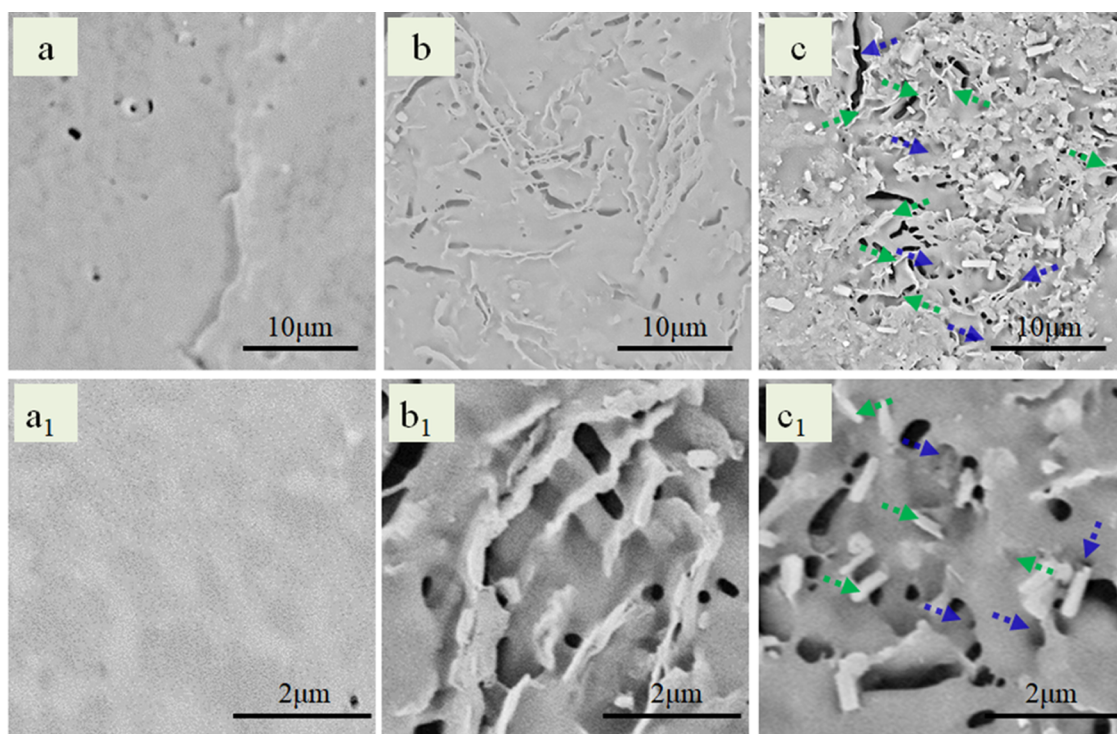

Figure 7. SEM images of the fractured surfaces of different scaffold samples: PLPC (a, a₁), PLPC/GO@DA (b, b₁), and PLPC/GO@nHA (c, c₁). Obviously, the PLPC sample showed a typical brittle fracture morphology with a relatively smooth and flat surface. For PLPC/GO@DA and PLPC/GO@nHA samples, the fractured surface showed partially exposed GO@DA sheets or staggered interconnected network structures, and there was also a microcrack structure caused by the pull-out effect.

surface area of GO provides a broad platform for the anchoring of ions. On the other hand, polydopamine formed by oxidative self-polymerization has various physical interactions, such as hydrogen bonding, $\pi-\pi$, electrostatic interactions, and so on. More importantly, it can catalyze the nucleation and growth of various inorganic nanoparticles and is well regarded as a mineralization inducer.[41] Under alkaline conditions, polydopamine shows the behavior of deprotonation to form oxygen anions. It can adsorb positively charged calcium ions (Ca^{2+}) through chelation and promote Ca^{2+} enrichment. Further, the anions in the solution are adsorbed by the electrostatic effect to induce the nucleation and in situ growth of nHA.

Therefore, under the synergistic effect of GO itself and DA, GO@DA can quickly induce the enrichment of Ca^{2+} in the precursor solution through the chelation of catechol groups and the adsorption behavior of −COOH or COO− groups, thereby forming a large number of nucleation sites (as shown in Figure 5a). Furthermore, the Ca^{2+} nucleation site will react in situ with anions such as PO_4^{3-} and CO_3^{2-} in the solution through electrostatic effects to promote the nucleation of nHA (Figure 5b). With the continuous deposition of ions under the effect of electrostatic adsorption, nHA rich in calcium and phosphorus will grow in situ on the surface of GO@DA, thereby obtaining the GO@nHA composite material (shown in Figure 5c). More importantly, by adjusting the concen-
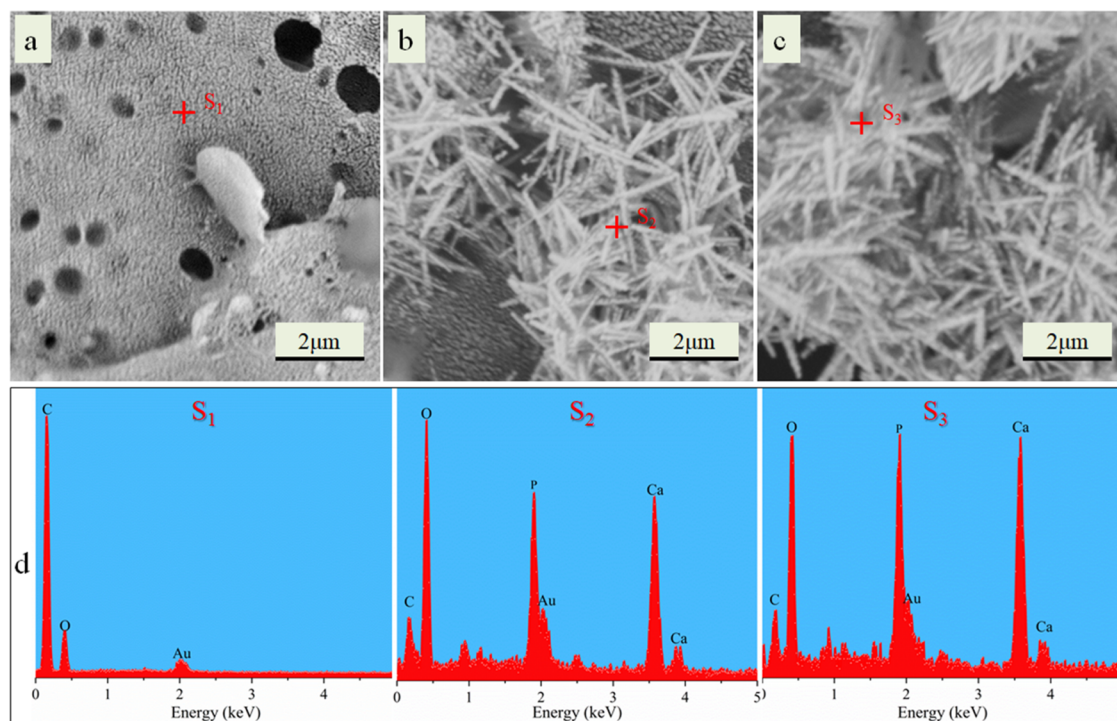
Figure 8. SEM surface morphologies of (a) PLPC, (b) PLPC/GO@DA, and (c) PLPC/GO@nHA scaffolds immersed in SBF for 21 days. (d) EDS point scanning spectra of S_1–S_3. Many needlelike Ca–P clusters were deposited on the surface of PLPC/GO@DA and PLPC/GO@nHA scaffolds, indicating that they have good apatite-forming ability.

tration of the reaction solution, the size, quantity, and even distribution of in situ nascent nHA can be controlled, which is expected to solve the problems of poor interfacial compatibility and uneven dispersion of multimaterials.[42] Therefore, exploring the dual effects of GO and DA to synergistically manipulate the biomimetic mineralization of graphene oxide and inorganic nanoparticles may be an effective and feasible method for preparing bone scaffold materials with excellent comprehensive properties.

3.5. Mechanical Properties of the Scaffold. The mechanical properties of different types of scaffolds were studied through compression tests, and the results are shown in Figure 6. It can be seen from the compressive stress–strain curve that three types of scaffold samples have similar stress change trends (Figure 6a). Among them, the ultimate strength of the PLPC sample was about 10.1 MPa. With the addition of GO@DA and GO@nHA, the ultimate strength was increased to 16.8 and 18.6 MPa, respectively, which is 66 and 84% higher than that of the PLPC scaffold. Moreover, the compressive modulus increased by 34 and 58% (from 128 MPa of PLA to 171 and 202 MPa), respectively. These results demonstrated that the addition of GO@DA and GO@nHA was beneficial to enhance the mechanical properties of polymer scaffolds. For PLPC/GO@DA scaffolds, the following factors might be responsible for the enhancement of mechanical properties. First, GO is a high-stiffness nanofiller that can physically enhance the mechanical properties of composites. Second, the high specific surface area of GO can significantly increase the contact area with the polymer matrix, thereby accelerating stress transfer.[43] Furthermore, DA modification allows GO and the polymer to be combined through chemical bonds, significantly enhancing the interaction of the contact interface. For PLPC/GO@nHA, in addition to the aforementioned factors, nHA is not only tightly combined with GO but also

can be pinned in the polymer matrix, thereby further improving the mechanical properties of composite scaffolds.[44]

To further explore the possible mechanism of mechanical performance improvement, the fracture morphology of scaffolds was observed by SEM, as shown in Figure 7. Obviously, the PLPC sample showed typical brittle fracture morphology with a relatively smooth and flat surface (Figure 7a). When 2 wt % GO@DA was added, the fracture morphology was still brittle, except for these nanosheets embedded in the matrix (Figure 7b). Interestingly, in the fracture surface of the scaffold containing GO@DA, some interconnected porous network structures were found, as shown in Figure 7b$_1$. This phenomenon indicated that the locally interconnected porous structure formed during dopamine modification was well preserved during the laser sintering process, which might be a factor in improving the mechanical properties of scaffolds. The fracture surface morphology of the GO@nHA sample is shown in Figure 7c,c$_1$, in which a certain degree of ductile fracture morphology was observed. Specifically, part structure of GO@DA and GO@nHA was exposed outside the polymer substrate, showing a typical pull-out effect (indicated by the green arrows). Correspondingly, the grooves or microcrack structures produced by the pull-out effect were also obvious (indicated by the blue arrows). In addition, traces of nHA appeared on the fracture surface, which may be caused by the pull-out effect during the fracture process. Meanwhile, some fine pores were found on the fracture surface of the PLPC/GO@nHA sample, which might be caused by nHA particles being pulled out. These results revealed that the in situ grown nHA and GO have a good interface bond and, to a certain extent, altered the fracture mode of composites. The transition of the fracture mode may be one of the factors for the improvement of the mechanical properties of scaffolds.
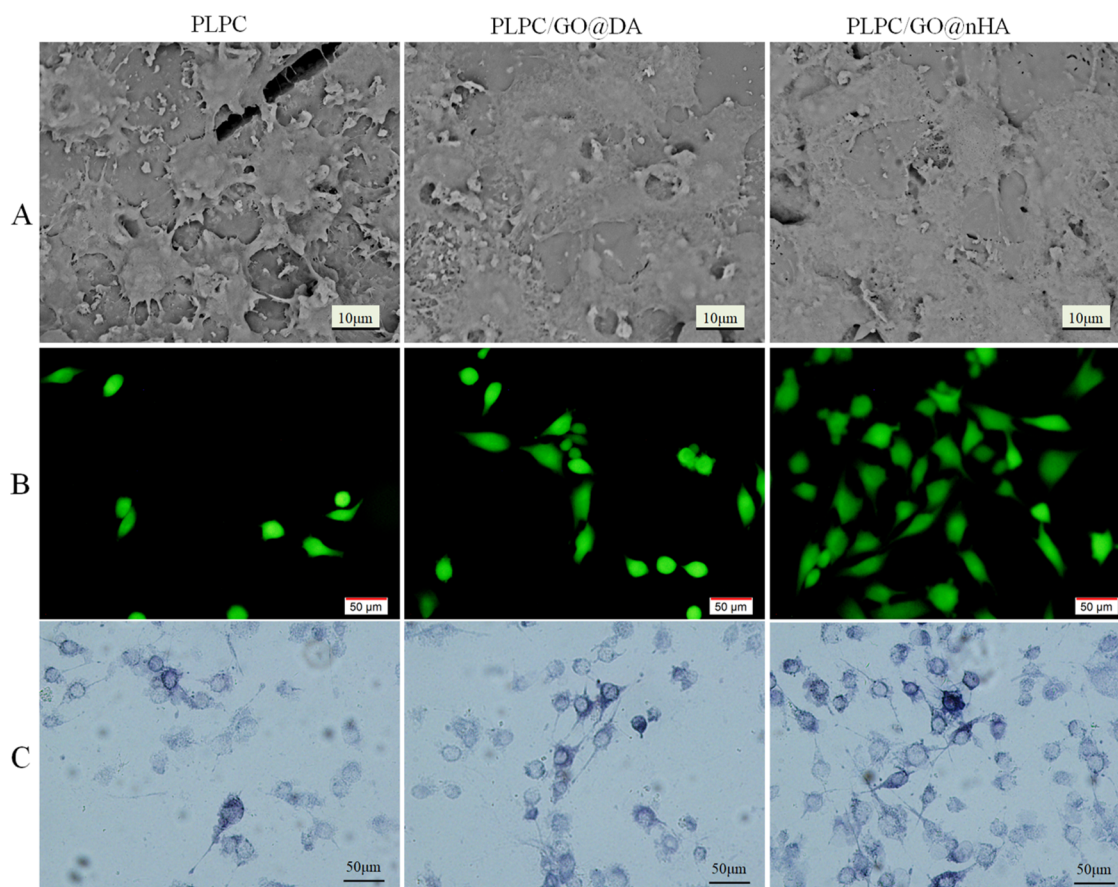
Figure 9. Adhesion morphology and viability of MG63 cells cultured on different scaffold samples for 24 h. (A) SEM image of cell adhesion morphology. Scaffolds containing GO@DA and GO@nHA could promote cell adhesion. (B) Immunofluorescence image for cell viability evaluation. Live/dead staining showed that most of the attached cells were vibrant (green). (C) Alkaline phosphatase (ALP) activity staining of cells cultured for 3 days.

3.6. Evaluation of Biomineralization Ability. The ability of the bone scaffold to induce bonelike apatite formation in the human environment is a prerequisite for evaluating whether it can form a biological bond with natural bone. Therefore, the prepared three types of scaffolds all performed the ability to form bonelike apatite in a simulated body fluid environment, and the results are shown in Figure 8. After 21 days of culture, some uneven small holes appeared on the surface of the PLPC scaffold, which may be caused by the hydrolysis of PLA and the shedding of sintered particles in the simulated body fluid environment (Figure 8a). However, there were almost no traces of bonelike apatite detected on the PLPC scaffold, which can be confirmed by EDS at the S_1 spot (no signs of Ca and P). These results indicated that the PLPC scaffold was limited in inducing apatite formation. In contrast, under the same culture conditions, PLPC/GO@DA and PLPC/GO@nHA scaffolds showed needlelike mineral deposits, as shown in Figure 8b,c. Furthermore, the presence of Ca and P elements in the EDS point scan pattern at S_2 and S_3 confirmed that these deposited minerals are Ca−P clusters. Moreover, it appears that the Ca−P clusters deposited on the PLPC/GO@nHA scaffold form a stack due to the increase in amount and density (Figure 8c). These results indicated that the PLPC/GO@nHA scaffold has the ability to induce apatite formation, which is expected to form a biological bond with natural bone after implantation.

3.7. Cytocompatibility Evaluation. The adhesion and proliferation of cells on the surface of the scaffold is an important prerequisite for the implant to induce bone repair. The cytocompatibility of the scaffold material was evaluated by adhesion morphology and viability of MG63 cells after 24 h of culture, and the results are shown in Figure 9. From the SEM micrograph in Figure 9A, the adherent cells on the PLPC sample exhibited a good adhesion state, but the spreading morphology of cells was not ideal, and the filopodia between cells were only rarely intertwined. In comparison, the cells were almost completely stretched and laid flat on the PLPC/GO@DA scaffold, and filopodia were interlaced with each other, which is very beneficial for the communication between cells. For the PLPC/GO@nHA scaffold, a cell layer has been formed due to the adhesion and flattening of a large number of cells, almost completely covering the entire surface of the scaffold. The cell adhesion morphology strongly indicated that the scaffold material in this study not only has no negative effects on the cells but also promotes the spread of cell adhesion.

The immunofluorescence experiment of preliminary cell culture using MG63 showed that all scaffold samples had high cell viability, as shown in Figure 9B. It was noticed that the living cells on the PLPC scaffold were mainly ellipsoidal, and only a small number of cells have traces of filopodia. In comparison, with the addition of GO@DA and GO@nHA, more cells present a flat shape with filopodia attached. At the

same time, the number of surviving cells (green fluorescent dots) on the scaffold seems to be increasing, and individual cells were growing larger. The increase in cell filopodia, number, and area might be due to the mitosis and proliferation of these cells. In addition, due to the increase in cell density, the larger green fluorescent dots may also be two or more cells clustered together. In general, the results of immunofluorescence experiments further showed that the prepared scaffold materials can effectively promote cell proliferation behavior. After 3 days, the ALP activity of the cultured cells was assessed, and the results are shown in Figure 9C. It can be seen that under the same culture conditions, with the addition of GO@ DA and GO@nHA, the stained cells exhibited a darker purple color, which corresponds to the increase in cellular ALP activity. Considering that the level of ALP activity is one of the indicators for evaluating the early differentiation of cells, it is reasonable to believe that the materials used in the development of composite scaffolds have a positive effect on stimulating cell differentiation. This may be attributed to the synergistic stimulation of cellular gene expression and mineralization by GO and in situ grown nHA, further inducing osteoblast differentiation.

The compositions and surface properties of biomaterials are important factors affecting the cell−biomaterial interaction. The differences in the morphology and number of cell adhesion on different samples may be attributed to the following aspects. First, the large specific surface area of GO@ DA and the structural defects introduced during the functionalization process may provide more cell adhesion sites on the surface of the scaffold.[45] Second, the wrinkled texture of GO@DA due to local redox and the porous structure formed by assembly may provide the surface of the scaffold with a micro−nanomorphology that is conducive to cell response.[46] For the PLPC/GO@nHA scaffold, in addition to the above factors, in situ growth nHA has a composition and structure similar to the inorganic components of natural bone,[47,48] thereby further inducing cell adhesion and stimulating cell proliferation.

4. CONCLUSIONS

In short, GO@nHA hybrid particles were prepared by combining effective organic modification and hydrothermal methods, and composite scaffolds containing these hybrid particles were constructed through a laser additive manufacturing process. Among them, GO@nHA was used to strengthen scaffolds and improve biological performance. Dopamine was used to construct GO@DA particles with a porous structure and induce nHA to grow in situ on the particles. The compression performance test results of the prepared scaffold showed that the composite scaffold has significantly enhanced mechanical properties. In addition, the good cytocompatibility of the prepared scaffold was confirmed by the adhesion and proliferation experiments of MG63 cells. All of these characteristics indicated that GO@nHA has the potential to be used as a bone scaffold material, and the PLPC/GO@nHA scaffold may be a potential candidate for the treatment of bone defects.

■ AUTHOR INFORMATION

Corresponding Authors

Mengqi Li − *Key Laboratory of Hunan Province for Efficient Power System and Intelligent Manufacturing, College of Mechanical and Energy Engineering, Shaoyang University, Shaoyang 422000, China*; Email: sciencefield@163.com

Yong Xu − *Key Laboratory of Hunan Province for Efficient Power System and Intelligent Manufacturing, College of Mechanical and Energy Engineering, Shaoyang University, Shaoyang 422000, China*; ◉ orcid.org/0000-0002-2511-638X; Email: xuyong2927@hnsyu.edu.cn

Authors

Dongying Li − *Key Laboratory of Hunan Province for Efficient Power System and Intelligent Manufacturing, College of Mechanical and Energy Engineering, Shaoyang University, Shaoyang 422000, China*

Meigui Chen − *Key Laboratory of Hunan Province for Efficient Power System and Intelligent Manufacturing, College of Mechanical and Energy Engineering, Shaoyang University, Shaoyang 422000, China*

Wenmin Guo − *Key Laboratory of Hunan Province for Efficient Power System and Intelligent Manufacturing, College of Mechanical and Energy Engineering, Shaoyang University, Shaoyang 422000, China*

Pin Li − *Key Laboratory of Hunan Province for Efficient Power System and Intelligent Manufacturing, College of Mechanical and Energy Engineering, Shaoyang University, Shaoyang 422000, China*

Haoyu Wang − *Key Laboratory of Hunan Province for Efficient Power System and Intelligent Manufacturing, College of Mechanical and Energy Engineering, Shaoyang University, Shaoyang 422000, China*

Wenhao Ding − *Key Laboratory of Hunan Province for Efficient Power System and Intelligent Manufacturing, College of Mechanical and Energy Engineering, Shaoyang University, Shaoyang 422000, China*

Complete contact information is available at:
https://pubs.acs.org/10.1021/acsomega.2c00629

Author Contributions

[†]D.L. and M.C. contributed equally to this work. D.L.: conceptualization, writing—review and editing, funding acquisition. M.C.: writing—review and editing. W.G.: conceptualization, methodology, supervision. H.W.: biomineralized experiment. P.L.: preparation of functionalized graphene oxide. W.D.: laser sintering test. M.L.: project administration, funding acquisition. Y.X.: methodology, investigation, writing—original draft, funding acquisition.

Notes

The authors declare no competing financial interest.

■ ACKNOWLEDGMENTS

■ REFERENCES

(1) García-Gareta, E.; Coathup, M. J.; Blunn, G. W. Osteoinduction of bone grafting materials for bone repair and regeneration. *Bone* **2015**, *81*, 112−121.

(2) Chen, X.; Chen, G.; Wang, G.; Zhu, P.; Gao, C. Recent Progress on 3D-Printed Polylactic Acid and Its Applications in Bone Repair. *Adv. Eng. Mater.* **2020**, *22*, No. 1901065.

(3) Tan, L.; Yu, X.; Wan, P.; Yang, K. Biodegradable materials for bone repairs: a review. *J. Mater. Sci. Technol.* **2013**, *29*, 503−513.

(4) Oliveira, H. L.; Da Rosa, W. L.; Cuevas-Suárez, C. E.; Carreno, N. L.; da Silva, A. F.; Guim, T. N.; Dellagostin, O. A.; Piva, E. Histological evaluation of bone repair with hydroxyapatite: a systematic review. *Calcif. Tissue Int.* **2017**, *101*, 341−354.

(5) Afroze, J. D.; Abden, M. J.; Islam, M. A. An efficient method to prepare magnetic hydroxyapatite−functionalized multi-walled carbon nanotubes nanocomposite for bone defects. *Mater. Sci. Eng. C* **2018**, *86*, 95−102.

(6) Lu, J.; Sun, C.; Yang, K.; Wang, K.; Jiang, Y.; Tusiime, R.; Yang, Y.; Fan, F.; Sun, Z.; Liu, Y.; et al. Properties of polylactic acid reinforced by hydroxyapatite modified nanocellulose. *Polymers* **2019**, *11*, No. 1009.

(7) Zhang, R.; Hu, H.; Liu, Y.; Tan, J.; Chen, W.; Ying, C.; Liu, Q.; Fu, X.; Hu, S.; Wong, C. P. Homogeneously dispersed composites of hydroxyapatite nanorods and poly (lactic acid) and their mechanical properties and crystallization behavior. *Composites, Part A* **2020**, *132*, No. 105841.

(8) Liu, C.; Huang, X.; Wu, Y. Y.; Deng, X.; Liu, J.; Zheng, Z.; Hui, D. Review on the research progress of cement-based and geopolymer materials modified by graphene and graphene oxide. *Nanotechnology* **2020**, *9*, 155−169.

(9) Ye, Y.; Chen, H.; Zou, Y.; Zhao, H. Study on self-healing and corrosion resistance behaviors of functionalized carbon dot-intercalated graphene-based waterborne epoxy coating. *J. Mater. Sci. Technol.* **2021**, *67*, 226−236.

(10) Li, M.; Xiong, P.; Yan, F.; Li, S.; Ren, C.; Yin, Z.; Li, A.; Li, H.; Ji, X.; Zheng, Y.; et al. An overview of graphene-based hydroxyapatite composites for orthopedic applications. *Bioact. Mater.* **2018**, *3*, 1−18.

(11) Ege, D.; Kamali, A. R.; Boccaccini, A. R. Graphene oxide/polymer-based biomaterials. *Adv. Eng. Mater.* **2017**, *19*, No. 1700627.

(12) Adnan, M. M.; Dalod, A. R.; Balci, M. H.; Glaum, J.; Einarsrud, M.-A. In situ synthesis of hybrid inorganic−polymer nanocomposites. *Polymers* **2018**, *10*, No. 1129.

(13) Costa, P. M.; Learmonth, D. A.; Gomes, D. B.; Cautela, M. P.; Oliveira, A. C.; Andrade, R.; Espregueira-Mendes, J.; Veloso, T. R.; Cunha, C. B.; Sousa, R. A. Mussel-Inspired Catechol Functionalisation as a Strategy to Enhance Biomaterial Adhesion: A Systematic Review. *Polymers* **2021**, *13*, No. 3317.

(14) Schindler, S.; Bechtold, T. Mechanistic insights into the electrochemical oxidation of dopamine by cyclic voltammetry. *Electroanal. Chem.* **2019**, *836*, 94−101.

(15) Umek, N.; Geršak, B.; Vintar, N.; Šoštarič, M.; Mavri, J. Dopamine autoxidation is controlled by acidic pH. *Front. Mol. Neurosci.* **2018**, *11*, No. 467.

(16) Xu, J.; Cheng, X.; Chen, F.; Li, W.; Xiao, X.; Lai, P.; Xu, G.; Xu, L.; Pan, Y. Fabrication of multifunctional polydopamine-coated gold nanobones for PA/CT imaging and enhanced synergistic chemo-photothermal therapy. *J. Mater. Sci. Technol.* **2021**, *63*, 97−105.

(17) Qiu, W.-Z.; Yang, H.-C.; Xu, Z.-K. Dopamine-assisted co-deposition: an emerging and promising strategy for surface modification. *Adv. Colloid Interfaces* **2018**, *256*, 111−125.

(18) Sun, N.; Jia, Y.; Wang, C.; Xia, J.; Dai, L.; Li, J. Dopamine-Mediated Biomineralization of Calcium Phosphate as a Strategy to Facilely Synthesize Functionalized Hybrids. *J. Phys. Chem. Lett.* **2021**, *12*, 10235−10241.

(19) Liu, L.; Meng, Y.; Dong, C.; Yan, Y.; Volinsky, A. A.; Wang, L.-N. Initial formation of corrosion products on pure zinc in simulated body fluid. *J. Mater. Sci. Technol.* **2018**, *34*, 2271−2282.

(20) Merlen, A.; Buijnsters, J. G.; Pardanaud, C. A guide to and review of the use of multiwavelength Raman spectroscopy for characterizing defective aromatic carbon solids: From graphene to amorphous carbons. *Coatings* **2017**, *7*, No. 153.

(21) Muzyka, R.; Drewniak, S.; Pustelny, T.; Chrubasik, M.; Gryglewicz, G. Characterization of graphite oxide and reduced graphene oxide obtained from different graphite precursors and oxidized by different methods using Raman spectroscopy. *Materials* **2018**, *11*, No. 1050.

(22) Bhaskaram, D. S.; Govindaraj, G. Carrier transport in reduced graphene oxide probed using Raman spectroscopy. *J. Phys. Chem. C* **2018**, *122*, 10303−10308.

(23) Jayavardhini, B.; Pravin, Y. R.; Kumar, C.; Murugesan, R.; Vedakumari, S. W. Graphene oxide impregnated sericin/collagen scaffolds−Fabrication and characterization. *Mater. Lett.* **2022**, *307*, No. 131060.

(24) Liu, Y.; Gan, D.; Chen, M.; Ma, L.; Yang, B.; Li, L.; Zhu, M.; Tu, W. Bioinspired dopamine modulating graphene oxide nano-composite membrane interposed by super-hydrophilic UiO-66 with enhanced water permeability. *Sep. Purif. Technol.* **2020**, *253*, No. 117552.

(25) Stroe, M. S.; Daescu, M.; Cercel, R.; Mogos, A.; Dragoman, D.; Socol, M.; Mercioniu, I.; Baibarac, M.; et al. Reduced Graphene Oxide Sheets as Inhibitors of the Photochemical Reactions of α-Lipoic Acid in the Presence of Ag and Au Nanoparticles. *Nanomaterials* **2020**, *10*, No. 2238.

(26) de Souza, C. B.; Nakagawa, M. A.; Vargas, L. R.; Hilario, R. B.; Impère, A. G. D.; Matsushima, J. T.; Quirino, S. F.; Gama, A. M.; Baldan, M. R.; Goncalves, E. S. Evolution of dielectric properties of thermally reduced graphene oxide as a function of pyrolisis temperature. *Diamond Relat. Mater.* **2019**, *93*, 241−251.

(27) Al-Gaashani, R.; Najjar, A.; Zakaria, Y.; Mansour, S.; Atieh, M. XPS and structural studies of high quality graphene oxide and reduced graphene oxide prepared by different chemical oxidation methods. *Ceram. Int.* **2019**, *45*, 14439−14448.

(28) Zeng, J.; Liu, Y.; Han, D.; Yu, B.; Deng, S.; Chen, F.; Fu, Q. Mechanical property enhancement of high conductive reduced graphene oxide fiber by a small loading of polydopamine. *Mater. Res. Express* **2018**, *5*, No. 045602.

(29) Zhu, X.; Yan, Q.; Cheng, L.; Wu, H.; Zhao, H.; Wang, L. Self-alignment of cationic graphene oxide nanosheets for anticorrosive reinforcement of epoxy coatings. *Chem. Eng. J.* **2020**, *389*, No. 124435.

(30) Xu, X.; Zheng, Q.; Bai, G.; Song, L.; Yao, Y.; Cao, X.; Liu, S.; Yao, C. Polydopamine induced in-situ growth of Au nanoparticles on reduced graphene oxide as an efficient biosensing platform for ultrasensitive detection of bisphenol A. *Electrochim. Acta* **2017**, *242*, 56−65.

(31) Zhu, X.; Zhao, H.; Wang, L.; Xue, Q. Bioinspired ultrathin graphene nanosheets sandwiched between epoxy layers for high performance of anticorrosion coatings. *Chem. Eng. J.* **2021**, *410*, No. 128301.

(32) Alkhouzaam, A.; Qiblawey, H.; Khraisheh, M. Polydopamine functionalized graphene oxide as membrane nanofiller: spectral and structural studies. *Membranes* **2021**, *11*, No. 86.

(33) Lu, Y.; Huang, L.; Guo, Y.; Yang, X. Theoretical insights into origin of graphene oxide acidity and relating behavior of oxygen-containing groups in water. *Carbon* **2021**, *183*, 355−361.

(34) Jebaranjitham, J. N.; Mageshwari, C.; Saravanan, R.; Mu, N. Fabrication of amine functionalized graphene oxide−AgNPs nano-composite with improved dispersibility for reduction of 4-nitrophenol. *Composites, Part B* **2019**, *171*, 302−309.

(35) Aradhana, R.; Mohanty, S.; Nayak, S. K. Comparison of mechanical, electrical and thermal properties in graphene oxide and reduced graphene oxide filled epoxy nanocomposite adhesives. *Polymer* **2018**, *141*, 109−123.

(36) Chen, G.; Wang, W.; Lu, X.; Mugaanire, I. T.; Zhang, Y.; Ai, Y.; Hou, K.; Hsiao, B. S.; Zhu, M. Homogeneous intercalated graphene/manganic oxide hybrid fiber electrode assembly by non-liquid-crystal spinning for wearable energy storage. *J. Mater. Sci. Technol.* **2022**, *97*, 1−9.

(37) Cao, N.; Lyu, Q.; Li, J.; Wang, Y.; Yang, B.; Szunerits, S.; Boukherroub, R. Facile synthesis of fluorinated polydopamine/chitosan/reduced graphene oxide composite aerogel for efficient oil/water separation. *Chem. Eng. J.* **2017**, *326*, 17−28.

(38) Deng, Y.; Liu, M.; Chen, X.; Wang, M.; Li, X.; Xiao, Y.; Zhang, X. Enhanced osteoinductivity of porous biphasic calcium phosphate

ceramic beads with high content of strontium-incorporated calcium-deficient hydroxyapatite. *J. Mater. Chem. B* **2018**, *6*, 6572−6584.

(39) Komai, S.; Hirano, M.; Ohtsu, N. Spectral analysis of Sr 3d XPS spectrum in Sr-containing hydroxyapatite. *Surf. Interface Anal.* **2020**, *52*, 823−828.

(40) Farokh Niaei, A. H.; Roman, T.; Hussain, T.; Searles, D. J. Computational study on the adsorption of sodium and calcium on edge-functionalized graphene nanoribbons. *J. Phys. Chem. C* **2019**, *123*, 14895−14908.

(41) Zhao, X.; Jia, N.; Cheng, L.; Liu, L.; Gao, C. Dopamine-induced biomimetic mineralization for in situ developing antifouling hybrid membrane. *J. Membr. Sci.* **2018**, *560*, 47−57.

(42) Zhu, Y.; Xu, L.; Liu, C.; Zhang, C.; Wu, N. Nucleation and growth of hydroxyapatite nanocrystals by hydrothermal method. *AIP Adv.* **2018**, *8*, No. 085221.

(43) Gong, L. X.; Pei, Y. B.; Han, Q. Y.; Zhao, L.; Wu, L. B.; Jiang, J. X.; Tang, L. C. Polymer grafted reduced graphene oxide sheets for improving stress transfer in polymer composites. *Compos. Sci. Technol.* **2016**, *134*, 144−152.

(44) Xue, X.-Z.; Zhang, J.-Y.; Zhou, D.; Liu, J.-K. In-situ bonding technology and excellent anticorrosion activity of graphene oxide/hydroxyapatite nanocomposite pigment. *Dyes Pigm.* **2019**, *160*, 109−118.

(45) Singh, D. P.; Herrera, C. E.; Singh, B.; Singh, S.; Singh, R. K.; Kumar, R. Graphene oxide: An efficient material and recent approach for biotechnological and biomedical applications. *Mater. Sci. Eng. C* **2018**, *86*, 173−197.

(46) Wang, B.; Song, Y.; Ge, L.; Zhang, S.; Ma, L. Antibody-modified reduced graphene oxide film for circulating tumor cell detection in early-stage prostate cancer patients. *RSC Adv.* **2019**, *9*, 9379−9385.

(47) Heshmatpour, F.; Haghbin, S. Nanohydroxyapatite/graphene oxide nanocomposites modified with synthetic polymers: promising materials for bone tissue engineering applications. *Int. J. Polym. Mater.* **2021**, *70*, 585−591.

(48) He, D.; Li, H. Biomaterials affect cell-cell interactions in vitro in tissue engineering. *J. Mater. Sci. Technol.* **2021**, *63*, 62−72.